Special Report 88-14

September 1988

US Army Corps of Engineers

Cold Regions Research & Engineering Laboratory

Eruptions from under-ice explosions

Malcolm Mellor and David L'Heureux

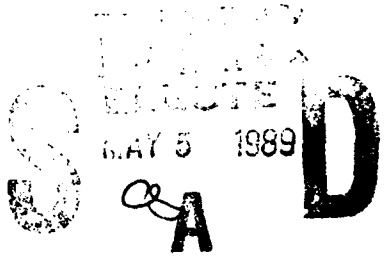

Prepared for
OFFICE OF THE CHIEF OF ENGINEERS

UNCLASSIFIED

SECURITY CLASSIFICATION OF THIS PAGE

REPORT DOCUMENTATION PAGE

Form Approved
OMB No. 0704-0188
Exp. Date: Jun 30, 1986

1a. REPORT SECURITY CLASSIFICATION
Unclassified

1b. RESTRICTIVE MARKINGS

2a. SECURITY CLASSIFICATION AUTHORITY

2b. DECLASSIFICATION / DOWNGRADING SCHEDULE

3. DISTRIBUTION / AVAILABILITY OF REPORT
Approved for public release; distribution is unlimited.

4. PERFORMING ORGANIZATION REPORT NUMBER(S)
Special Report 88-14

5. MONITORING ORGANIZATION REPORT NUMBER(S)

6a. NAME OF PERFORMING ORGANIZATION
U.S. Army Cold Regions Research and Engineering Laboratory

6b. OFFICE SYMBOL (If applicable)
CECRL

7a. NAME OF MONITORING ORGANIZATION
Office of the Chief of Engineers

6c. ADDRESS (City, State, and ZIP Code)
Hanover, New Hampshire 03755-1290

7b. ADDRESS (City, State, and ZIP Code)
Washington, D.C. 20314-1000

8a. NAME OF FUNDING / SPONSORING ORGANIZATION

8b. OFFICE SYMBOL (If applicable)

9. PROCUREMENT INSTRUMENT IDENTIFICATION NUMBER

8c. ADDRESS (City, State, and ZIP Code)

10. SOURCE OF FUNDING NUMBERS

PROGRAM ELEMENT NO.	PROJECT NO. 4A7627 30AT42	TASK NO. CS	WORK UNIT ACCESSION NO. 001

11. TITLE (Include Security Classification)
Eruptions from Under-Ice Explosions

12. PERSONAL AUTHOR(S)
Mellor, Malcolm and L'Heureux, David

13a. TYPE OF REPORT	13b. TIME COVERED FROM _____ TO _____	14. DATE OF REPORT (Year, Month, Day)	15. PAGE COUNT
		September 1988	28

16. SUPPLEMENTARY NOTATION

17. COSATI CODES		
FIELD	GROUP	SUB-GROUP

18. SUBJECT TERMS (Continue on reverse if necessary and identify by block number)
Eruptions
Explosions
Explosives
Ice penetration
Under-ice explosions
Underwater explosions

19. ABSTRACT (Continue on reverse if necessary and identify by block number)
Eruptions from under-ice explosions were recorded by a standard video camera and an ordinary motor-driven 35-mm camera. The records give the dimensions and velocities of the eruptions. Velocity, diameter, and height are related to charge depth and the results are compared with data for ordinary underwater explosions in ice-free water.

20. DISTRIBUTION / AVAILABILITY OF ABSTRACT
☒ UNCLASSIFIED/UNLIMITED ☐ SAME AS RPT. ☐ DTIC USERS

21. ABSTRACT SECURITY CLASSIFICATION
Unclassified

22a. NAME OF RESPONSIBLE INDIVIDUAL
Malcolm Mellor

22b. TELEPHONE (Include Area Code)
603-646-4100

22c. OFFICE SYMBOL
CECRL-EE

DD FORM 1473, 84 MAR

83 APR edition may be used until exhausted.
All other editions are obsolete.

SECURITY CLASSIFICATION OF THIS PAGE

UNCLASSIFIED

PREFACE

This report was prepared by Dr. Malcolm Mellor, Experimental Engineering Division, and David L'Heureux, Visual Information Branch, Information Management Division, U.S. Army Cold Regions Research and Engineering Laboratory.

Field data for this report were gathered during a winter bridging exercise with Echo Company, 2nd Engineer Battalion, in Korea. The field project was carried out under DA Project 4A762730AT42, *Design, Construction, and Operations Technology for Cold Regions*, Task CS, *Bridging Concepts*, Work Unit 001, *Cold Weather Bridging*. The report was prepared under the same project, Task CS, *Vehicular Barriers*, Work Unit 029, *Explosives and Projectile Impact Under Winter Conditions.*

The contents of this report are not to be used for advertising or promotional purposes. Citation of brand names does not constitute an official endorsement or approval of the use of such commercial products.

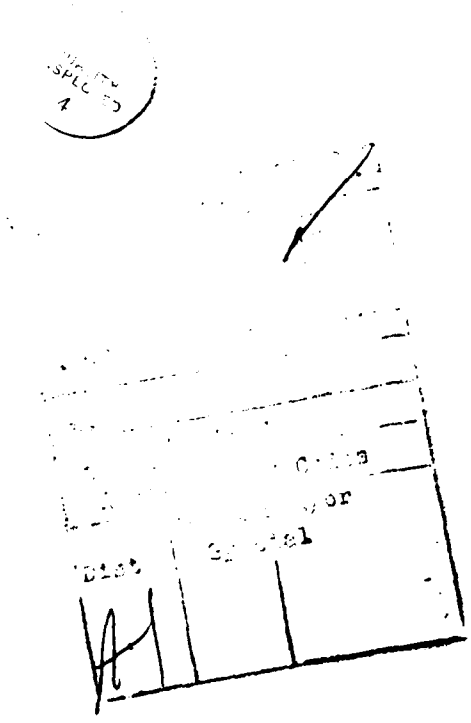

Eruptions from Under-Ice Explosions

MALCOLM MELLOR AND DAVID L'HEUREUX

INTRODUCTION

During a winter bridging study in Korea, underwater explosions were fired beneath a thin ice cover on the Imjin River. The resulting eruptions of water and ice fragments were recorded with a video camera and motor-driven 35-mm cameras. The video tapes and the photographs were used to measure the maximum diameter and height of each eruption, as well as the vertical velocity of the eruption.

The explosions were tests designed to establish procedures for ice-clearing, and consequently they were not ideal for studying the characteristics of the eruptions. However, they did provide some useful information in an area where data are lacking. The records and measurements also demonstrated that simple equipment, used as opportunity offers, is capable of producing good data.

Because the ice thickness was small relative to the size of the charges, these explosions in the Imjin River probably gave eruptions that are not much different from those produced by explosions beneath a free water surface.

TEST EXPLOSIONS

The primary objective of the work was to develop efficient blasting procedures for clearing a channel across an ice-covered river. Thus most of the tests involved multiple charges, with horizontal separation near the minimum for production of separate eruptions. The ice cover on the river was thin (< 9 in., or < 220 mm) and the individual charges were relatively large (5–40 lb, or 2.3–18 kg) to minimize the number required, and hence to simplify the blasting procedure. Current velocity in the river was very low, so that the charges hung vertically beneath the ice when inserted through drill holes. The river was quite shallow during the test period, so that scaled charge depths were necessarily limited, and charges sometimes rested on the river bed.

Each charge was inserted through a drill hole or through a hole cut with a chain saw. It was suspended at the required depth on a downline of detonating cord. The detonating cord was initiated on the ice surface by an electric blasting cap. Details of the explosions are given in Table 1, which also lists the size of the crater* that was blown through the ice surface by each explosion. A selection of time-sequence photographs is provided in Appendix A.

DATA FROM THE VIDEO CAMERA

The video camera was a Panasonic industrial camera, model 3250, with a Newvicon tube. The recording deck was a Panasonic portable video cassette recorder, model no. NV8429, using the VHS (half-inch tape) system. This was the standard equipment used for recording the general project operations.

The camera was aimed at the charge location and the lens was adjusted to give optimum coverage for the estimated height of the eruption. The camera had to be far enough back to avoid damage from flying debris. Wherever possible, the field of view was chosen to give a dark background (steep, wooded slopes of the riverbank), with any direct sunlight coming from behind the camera. A length scale was provided by laying out a line through the shot point and at right angles to the sight line; the ends of the measured line were marked by dark rocks laid on the ice.

Video taping started prior to the countdown for the blast and continued until after all the debris had finished falling. Tapes were reviewed immediately after each blast in order to make a qualitative assessment of the blast results.

Back in the laboratory, the tapes were run through an editor frame by frame. The height of

* Crater—the zone where the ice is fragmented and displaced, leaving open water or fragments that are not connected to the surrounding ice.

Table 1. Results of blasting tests on the Imjin River, 1987.

Shot no.	*Ice thickness (in.)*	*Water depth (ft)*	*Charge design*	*Blast effects*
1	7	9	3×5-lb charges of C-4 at 18-ft ctrs. Outer charges 2 ft below top of ice. Middle charge 3.3 ft below top of ice. No delays.	Crater length 61 ft. Crater width 28–29 ft (mean width 28.5 ft).
2	8	6.8	3×5-lb charges of C-4 at 18-ft ctrs. Outer charges 5.6 ft below top of ice. Middle charge 6.8 ft below top of ice (on river bed). No delays.	Crater length 65.5 ft. Crater width 32.5–36.5 ft (mean width 34.3 ft).
3	8	7	3×5-lb charges of C-4 at 18-ft ctrs. All charges 11.5 in. below top of ice (3.5 in. below base of ice). No delays.	Crater length 65.5 ft. Crater width 38.5–41 ft (mean width 39.7 ft).
4	8	9.9	40-lb charge of TNT, 7 ft below top of ice.	Crater diameter 58.3–59.3 ft (mean 58.8 ft).
5	8.5	—	12×5-lb charges, 3 rows, 20 ft between rows, 20 ft between charges in each row. All charges 2 ft below top of ice. Delays between rows. Zero for left row, 100 ms for center row, 200 ms for right row (see diagram).	Crater length 109 ft. Crater width 83 ft.
6	8.5	—	12×5-lb charges of TNT, 3 rows, 20 ft between rows, 20 ft between charges in each row. All charges 2 ft below top of ice. Delays between rows. Zero for outer rows, 200 ms for middle row (see diagram).	Crater length 97 ft. Crater width 77 ft.
7	8–8.5	—	5×40-lb charges of TNT. Single row with charges at 40-ft ctrs, 7 ft deep.	Crater width 56 ft fully fragmented, 98 ft well fractured with floes ≤3 ft.
8	7.5	—	40-lb charge of TNT and dynamite. 5 ft below top of ice.	

Table 2. Velocity measurements from video records.

	Initial velocity		*Second-stage velocity*			*Initial velocity*		*Second-stage velocity*	
Shot no.	*Velocity (ft/s)*	*Height range (ft)*	*Velocity (ft/s)*	*Height range (ft)*	*Shot no.*	*Velocity (ft/s)*	*Height range (ft)*	*Velocity (ft/s)*	*Height range (ft)*
1 left	215	< 57	—	—	5 left	260	< 40	193	43–75
1 right	232	< 58	—	—	4 right	274	< 40	173	48–76
1 middle	161	< 54	—	—	5 middle	272	< 55	194	55–74
2 left	108	< 14	44	15–30	6 left	268	<100	218	108–145
2 right	103	< 16	50	17–35	6 right	272	< 63	179	63–134
2 middle	162	< 15	29	18–30	6 middle	299	< 90	225	90–119
3 left	516	< 32	116	32–56	7 left outer	159	< 31	100	32–78
3 right	562	—	121	17–42	7 left inner	154	< 36	136	36–99
3 middle	556	< 36	100	36–62	7 middle	184	< 40	113	40–93
4	101	< 25	85	≈ 40	7 right inner	177	< 42	138	44–86
					7 right outer	152	< 42	114	42–70

Table 3. Measurements made from photographs.

Shot no.	Scaled ice thickness ($ft/lb^{1/3}$)	Scaled charge depth ($ft/lb^{1/3}$)	Max. diameter of column or plume		Max. height of column or jet		Approximate velocity	
			(ft)	($ft/lb^{1/3}$)	(ft)	($ft/lb^{1/3}$)	Velocity (ft/s)	Height range (ft)
1 left	0.34	1.17	12.7 (near base)	7.43	≈ 140	≈ 81.9	≥235	0–47
							316(jet)	47–110
1 right	0.34	1.17	12.0 (near base)	7.02	≈ 140	≈ 81.9	≥253	0–51
							298 (jet)	51–110
1 middle	0.34	1.93	11.4 (near base and mid-ht.)	6.67	94	55.0	≥108	0–22
							132	22–48
2 left	0.39	3.27	≈ 32	≈ 18.7	54	31.6	≥215	0–43
							63	43–56
2 right	0.39	3.27	≈ 22	≈ 12.9	50	29.9	≥226	0–45
							18	45–50
2 middle	0.39	3.98	—	—	47	27.5	≥188	0–38
							18	38–43
3 left	0.39	0.56	15.5 (near base)	9.06	149	87.1	≥286	0–57
			36 (smoke crown)	21.1			110	57–79
							124 (jet)	79–104
3 right	0.39	0.56	13.0 (near base)	7.60	130	76.0	≥268	0–54
			34 (smoke crown)	19.9			96	54–73
							101 (jet)	73–93
3 middle	0.39	0.56	13.9 (near base)	8.13	189	110.1	≥288	0–58
			—	—			170	58–93
							147 (jet)	93–122
4 (#1 camera)	0.19	2.05	27 (near base and at 36-ft ht.)	7.89	167	48.8	≥180	0–36
							204	36–77
							284 (jet)	77–134
4 (#2 camera)	0.19	2.05	26 (near base and at 33-ft ht.)	7.60	—	—	198	0–40
							140	40–68
6 left	0.41	1.17	16 (near base)	9.36	≈ 135	≈ 78.9	≥317	0–63
			16 (at 70-ft ht.)	9.36			248 (jet)	63–117
6 right	0.41	1.17	16 (near base)	9.36	≈ 129	≈ 75.4	≥298	0–60
			18 (at 67-ft ht.)	10.53			157 (jet)	60–94
6 middle	0.41	1.17	16 (near base)	9.36	≈ 127	≈ 74.3	≥277	14–71
			16 (at 68-ft ht.)	9.36				
7 left outer	0.18	2.05	31 (mid-ht.)	9.06	168	49.1	230	130–160
7 left inner	0.18	2.05	29 (mid-ht.)	8.48	189	55.3	275	130–160
7 middle	0.18	2.05	29 (mid-ht.)	8.48	207	60.5	283	130–160
7 right inner	0.18	2.05	29 (mid-ht.)	8.48	207	60.5	277	130–160
7 right outer	0.18	2.05	30 (mid-ht.)	8.77	173	50.6	211	130–160

each eruption was measured frame by frame on a 20-in. TV screen, so that graphs of height vs time could be plotted. The framing rate was 30/s so that the interval between successive measurements was 33.3 ms.

Results of the video measurements are shown graphically in Appendix B (Fig. B1–B9). Velocities were measured from these graphs, giving the results shown in Table 2.

The video tapes were not used to measure the maximum height and maximum diameter of the eruptions because still photographs from the motor-driven camera provided greater clarity and better contrast. The video images of the eruptions, which tend to have diffuse (fuzzy) edges, do not always show up clearly against snow-covered ice or against a light sky. The maximum height of the eruption was not always in the frame of view.

DATA FROM MOTOR-DRIVEN CAMERAS

The motor-driven cameras were ordinary SLR 35-mm cameras (Olympus OM-2) fitted with battery-powered drive units. With ordinary films of moderately high speed, there was no difficulty in operating at high shutter speeds, since the lighting was bright (typically sun on snow).

The camera was aimed at the shot points, including in the field of view the pair of rocks that

had been set at a measured distance apart on a line perpendicular to the sight line and through the shot point. The intention was to have two cameras recording each blast, one to give details of the initial stage of the eruption and the other to cover the complete height range of the eruption. However, one camera malfunctioned during most of the shots (the shutter jammed). The cameras were triggered manually on the countdown for the blast, which was fired electrically. Air temperatures were mild (usually slightly above freezing), and there were no indications that the cameras suffered from stiffening of lubricants or film.

Measurements were made on the resulting photographs to obtain the maximum diameter and the maximum height of each eruption. Table 3 gives these dimensions, and samples of the photographs are shown in Appendix A.

Wherever possible, the first two or three photographs in a sequence were used to obtain an estimate of vertical velocity from the height measurements. The nominal advance rate of the motor drives was 5 frames per second, giving a nominal time interval of 200 ms between exposures. The cameras and drive units were calibrated back at the laboratory at an appropriate temperature, and the actual framing intervals were found to be 204 ms for the camera that functioned continuously and 235 ms for the faulty camera. Both cameras reached steady speed after one frame; the faulty camera was very slow for the first frame but the other camera was only slightly below the rated speed for the first frame advance. The velocity estimates are given in Table 3.

Photo coverage of the blasts was incomplete. This was due partly to failure of one camera, as already mentioned, and partly because the explosions were triggered, either prematurely or late, by inexperienced troops using primitive equipment (the operation was also a training exercise for the troops).

DISCUSSION

The values listed in Table 2 as "initial velocity" are eruption velocities that actually apply over a large height range, mostly in excess of 5 m and in some cases over 17 m (Fig. B1–B9). These "initial velocities" should not be confused with the true initial velocities that are measured in the shock-induced spray domes from standard underwater explosions. Having stressed this distinction, the velocities from Table 2 are related to scaled charge depth (Table 4) and compared with theoretical

Table 4. Initial velocity and scaled charge depth.

Shot no.	*Scaled charge depth* ($ft/lb^{1/3}$)	*Initial vertical velocity from video records (ft/s)*	*Initial vertical velocity from motor-driven camera (ft/s)*
1 left outer	1.17	215	235
1 right	1.17	232	253
1 middle	1.93	161	108
2 left	3.27	108	215
2 right	3.27	103	268
2 middle	3.98	162	288
3 left	0.56	516	266
3 right	0.56	562	268
3 middle	0.56	556	288
4	2.05	101	180,198
5 left	1.17	260	—
5 right	1.17	274	—
5 middle	1.17	272	—
6 left	1.17	268	317
6 right	1.17	272	298
6 middle	1.17	299	—
7 left outer	2.05	159	—
7 left inner	2.05	154	—
7 middle	2.05	184	—
7 right inner	2.05	177	—
7 right outer	2.05	152	—

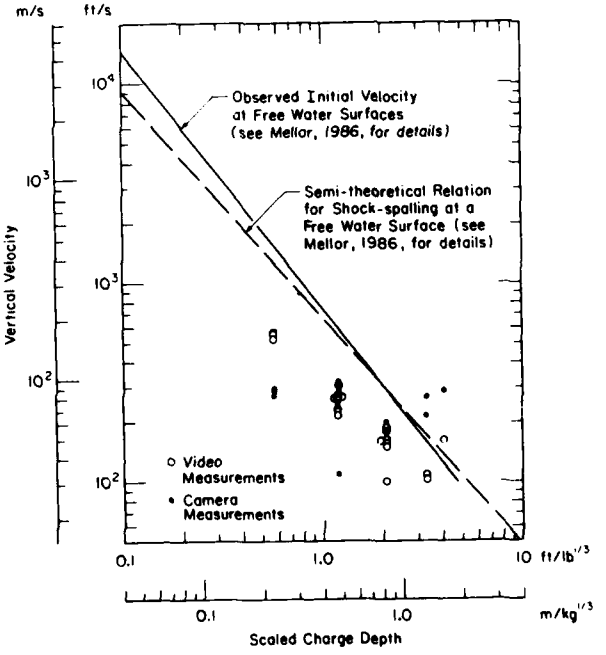

Figure 1. Initial vertical velocity plotted against scaled charge depth.

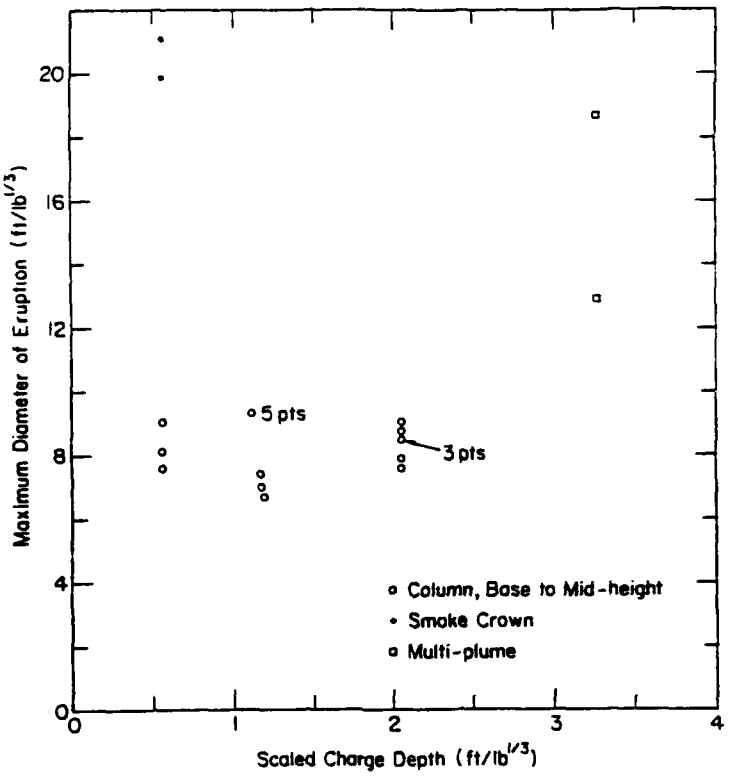

Figure 2. Scaled maximum diameter of the eruption plotted against scaled charge depth.

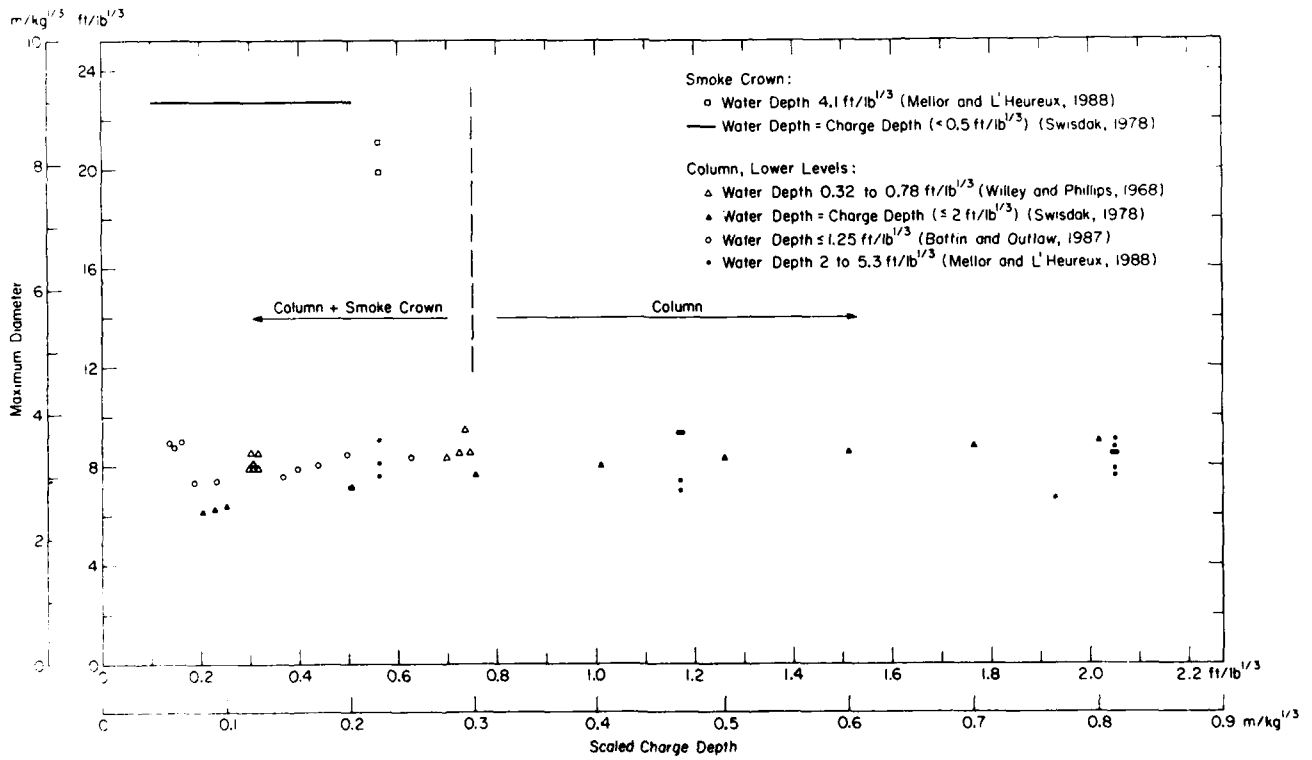

Figure 3. Comparison of diameter data with results for ice-free water.

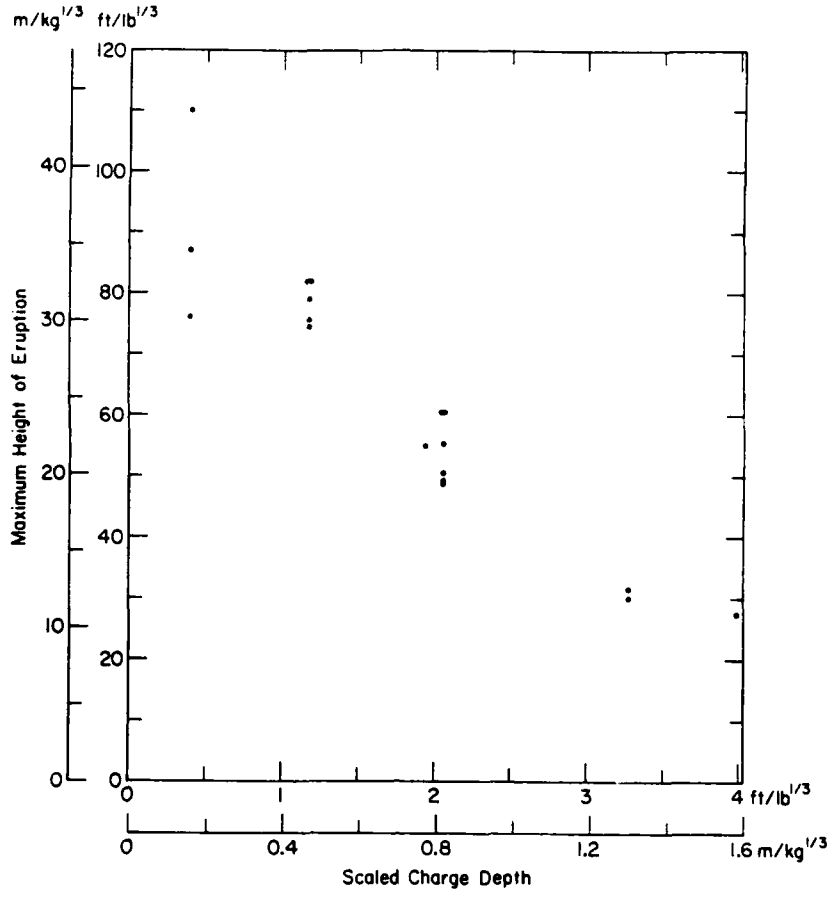

Figure 4. Scaled maximum height of the eruption plotted against scaled charge depth (using cube-root scaling for charge depth).

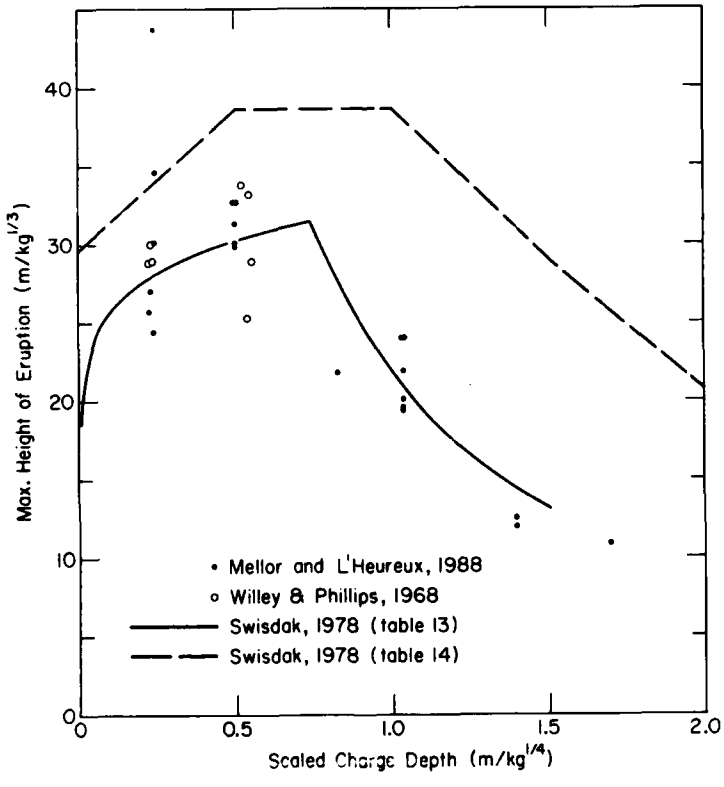

Figure 5. Comparison of height data with results for ice-free water (using fourth-root scaling for charge depth).

shock-spalling velocities for a free water surface and with observed initial velocities for ordinary underwater explosions (Fig. 1). The discrepancies between camera and video measurements in shots 2 and 3 have not been explained; one possibility is that the motor drive or the shutter malfunctioned.

For relatively large-scaled charge depths, the emergence velocities for the ice eruptions cluster around the trend lines for ejection velocities from free water surfaces. At smaller scaled charge depths, the observed emergence velocities for the ice eruptions were smaller than the initial vertical velocities on free water surfaces.

The diameter of the eruption, as given in Table 3, is shown graphically in Figure 2. Most of the eruptions were of columnar form, and the maximum diameters were in good agreement with comparable measurements made in shallow ice-free water (Fig. 3). One set of shallow-depth charges produced smoke crowns, for which the maximum diameters (Fig. 3) were not far from the values given by Swisdak (1978).

The maximum height of the eruption is plotted against charge depth in Figure 4. A comparison with comparable published data for ice-free water is given in Figure 5. Apart from two high values that were observed in shot 3, the agreement with data for ice-free water is good.

REFERENCES

Bottin, R.R. and D.G. Outlaw (1987) Explosion-generated waves in shallow water. USA Waterways Experiment Station, Miscellaneous Paper CERC-87-13.

Mellor, M. (1986) Blasting and blast effects in cold regions. Part II. Underwater explosions. USA Cold Regions Research and Engineering Laboratory, Special Report 86-16.

Swisdak, M.M. (1978) Explosion effects and properties. Part II. Explosion effects in water. Naval Surface Weapons Center, Technical Report 76-116.

Wiley, R.L. and D.E. Phillips (1968) Surface phenomena measurements and experimental procedures in 4000-lb HBX-1 shallow underwater explosive tests (Project "HEAT"). U.S. Naval Ordnance Laboratory, White Oak, Silver Spring, Maryland, NOLTR 68-74.

APPENDIX A: SELECTION OF PHOTOGRAPHS FROM MOTOR-DRIVEN CAMERAS

Within each sequence of photographs, the nominal interval between frames is 20 ms. The actual framing interval was 204 ms for all sequences except (3); for (e) the interval was 235 ms.

In most cases, frames from the end of the sequence are not shown here. The frames omitted are those where material is falling back from the highest levels.

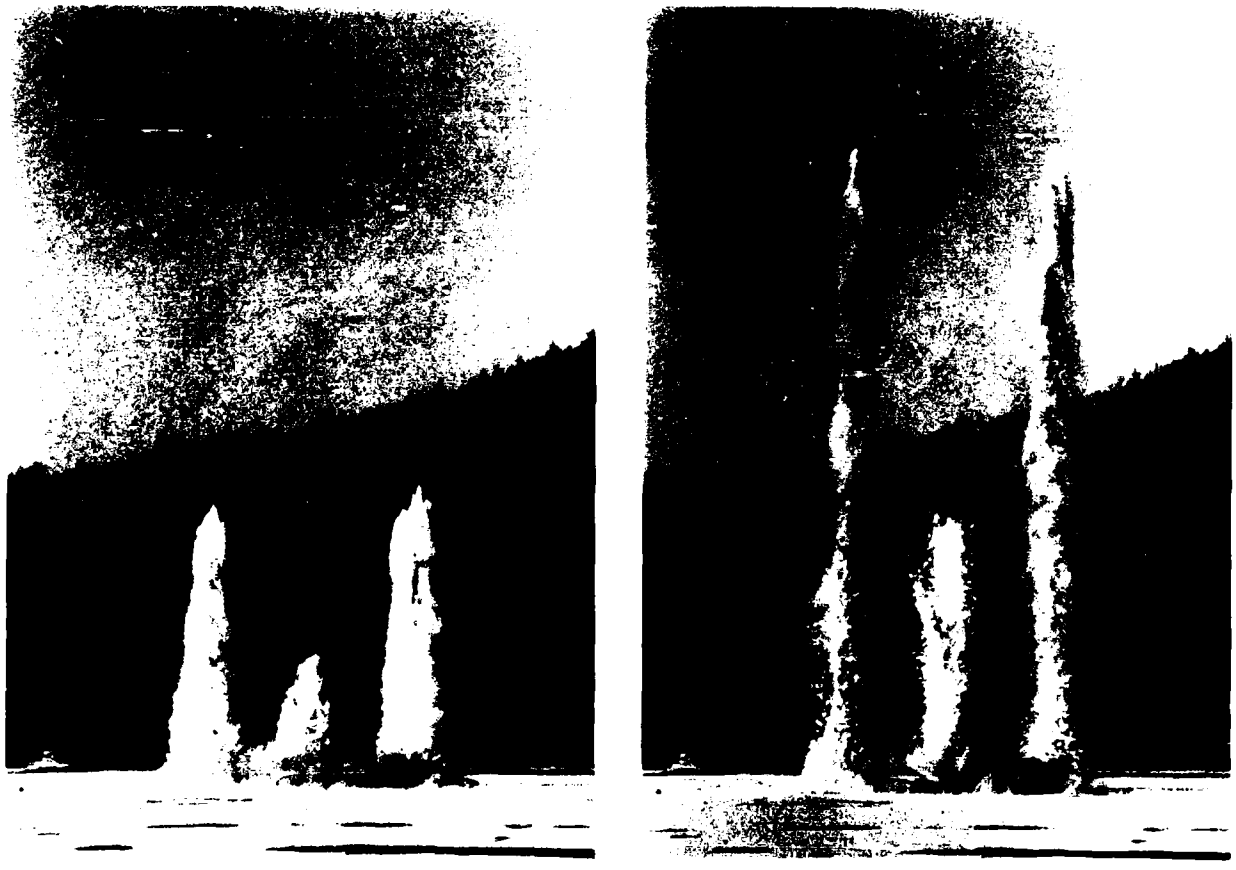

Figure A1. Six-frame sequence of shot no. 1 (2-second duration).

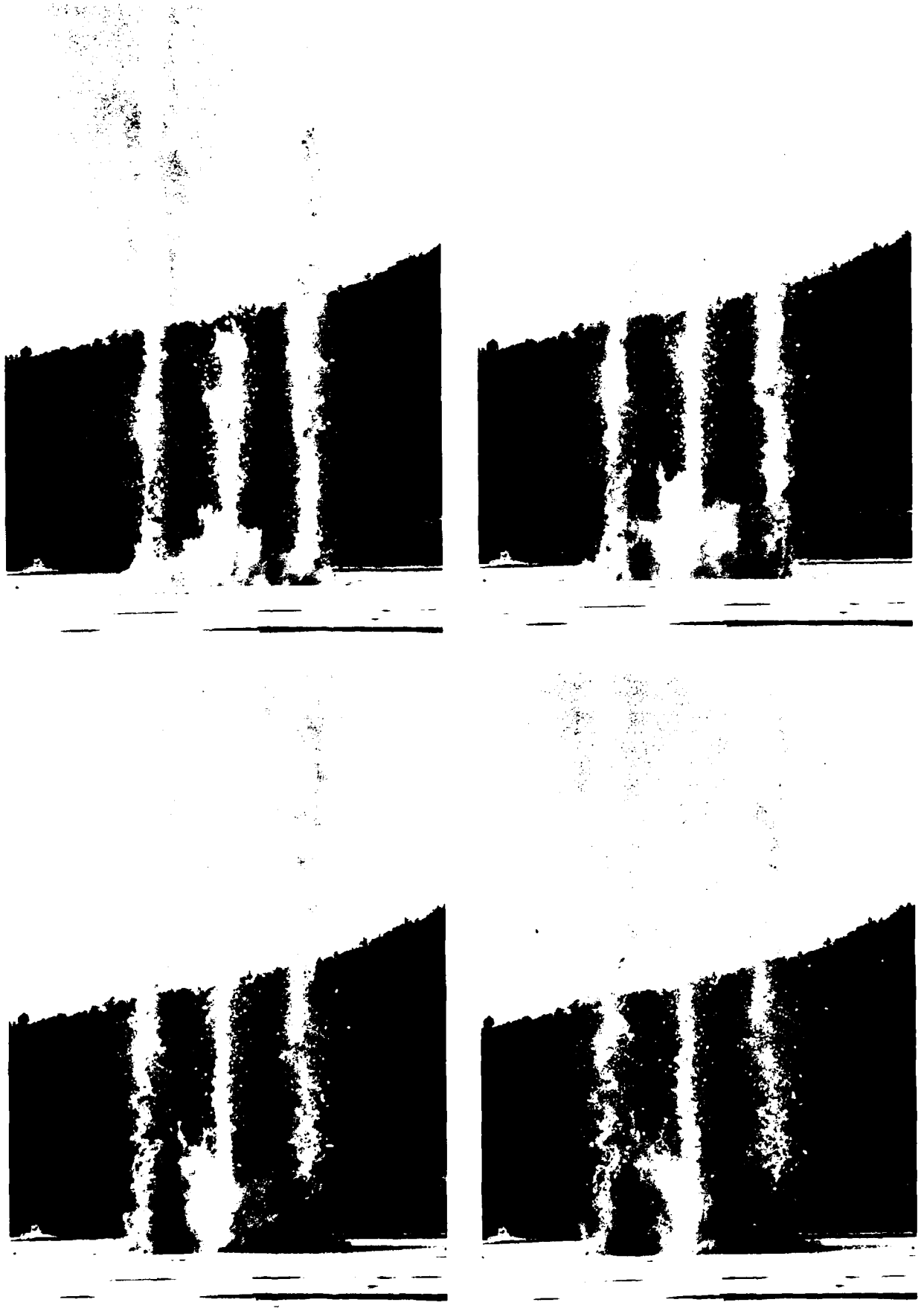

Figure A1 (cont'd). Six-frame sequence of shot no. 1 (2-second duration).

Figure A2. Three-frame sequence of shot no. 2.

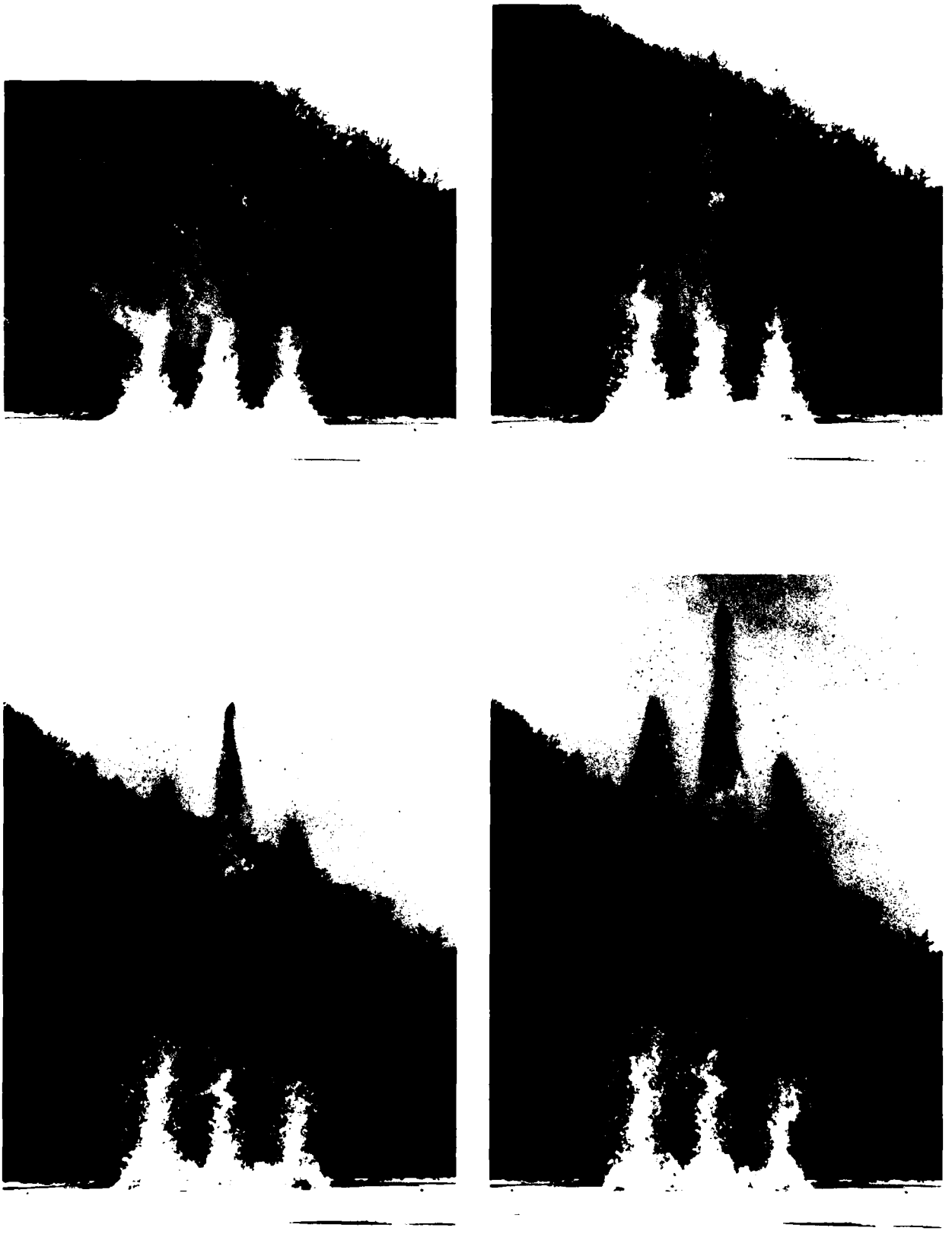

Figure A3. Six-frame sequence of shot no. 3.

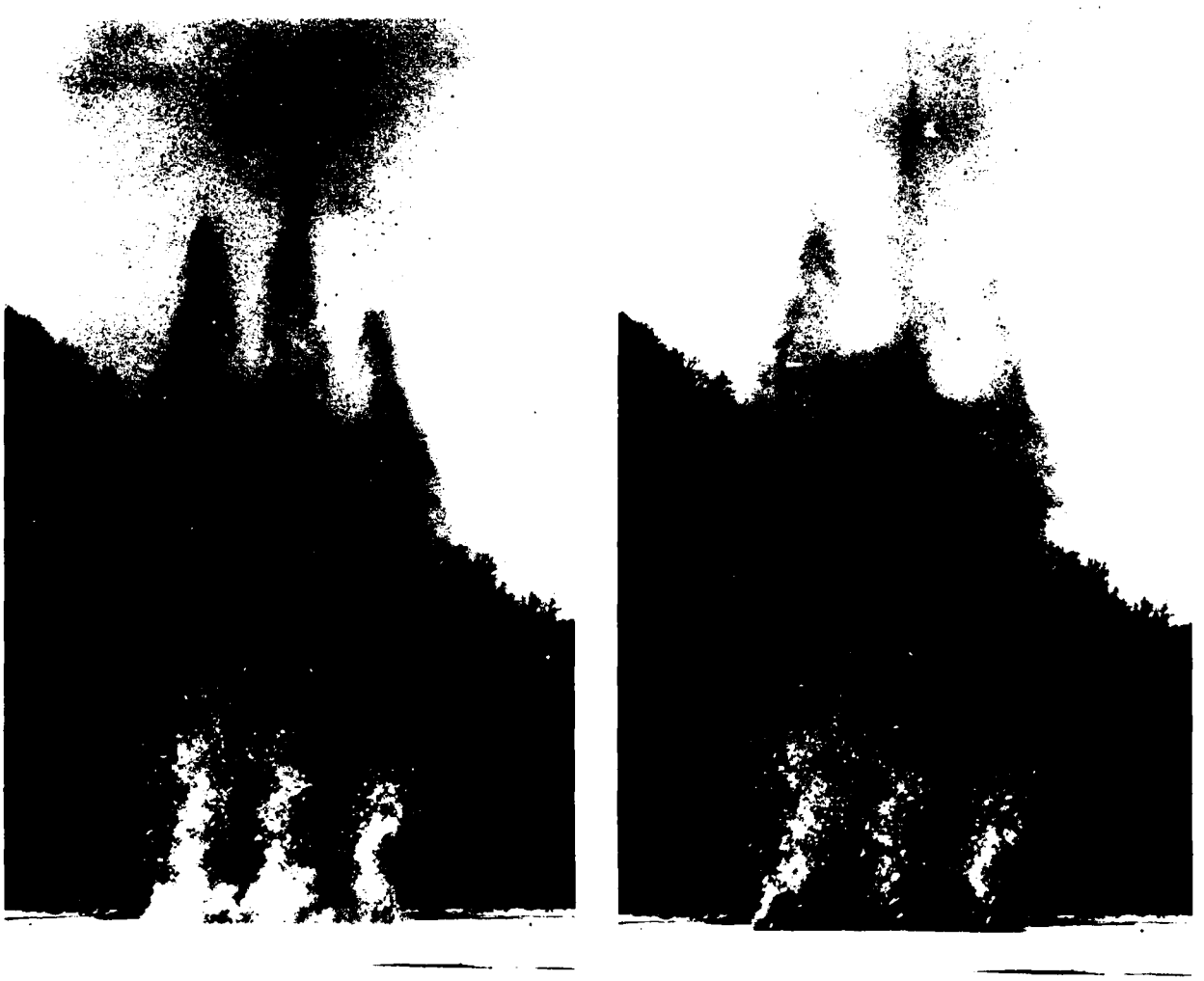

Figure A3 (cont').

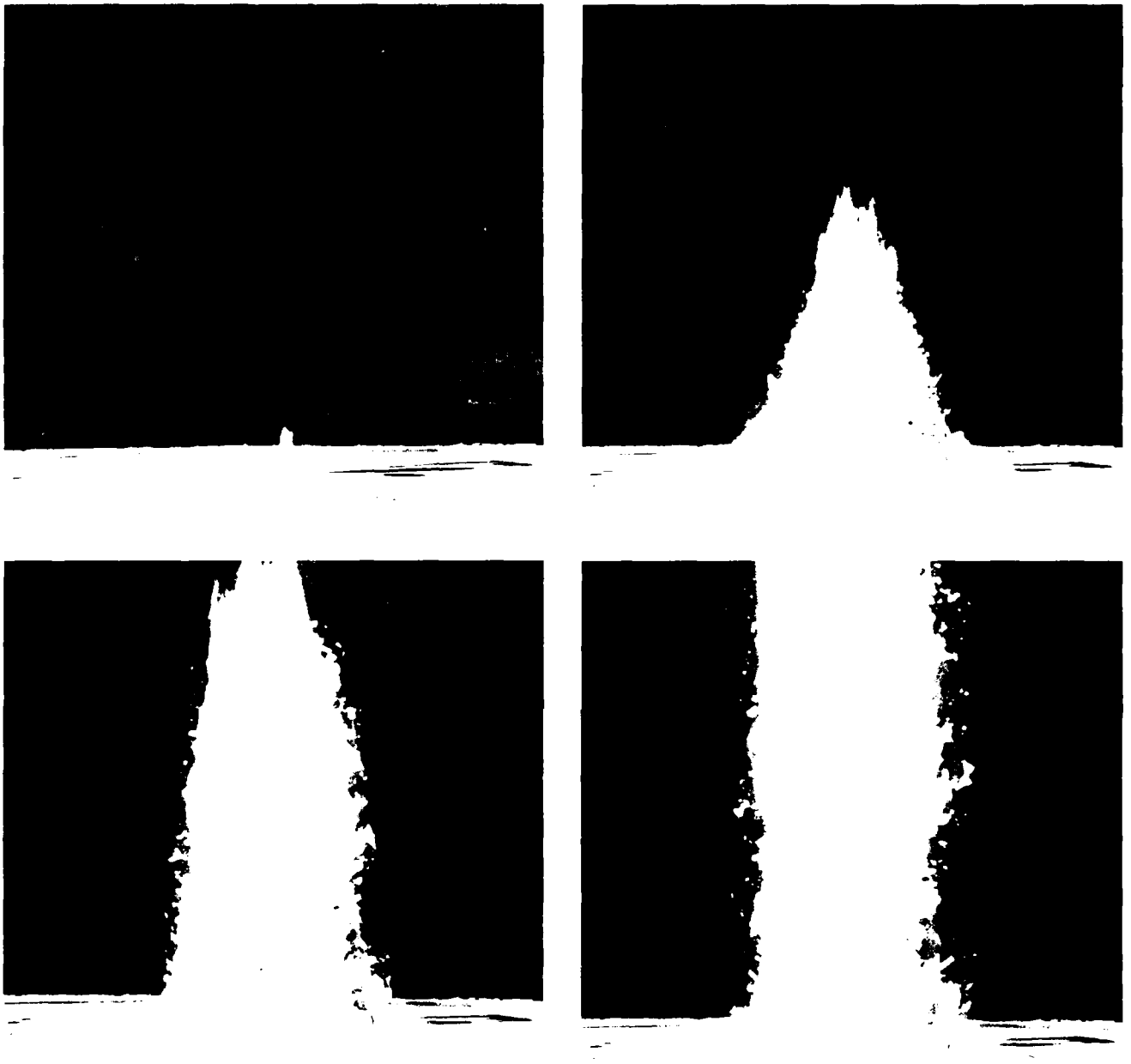

Figure A4. Six-frame sequence of shot no. 4 (camera no. 1).

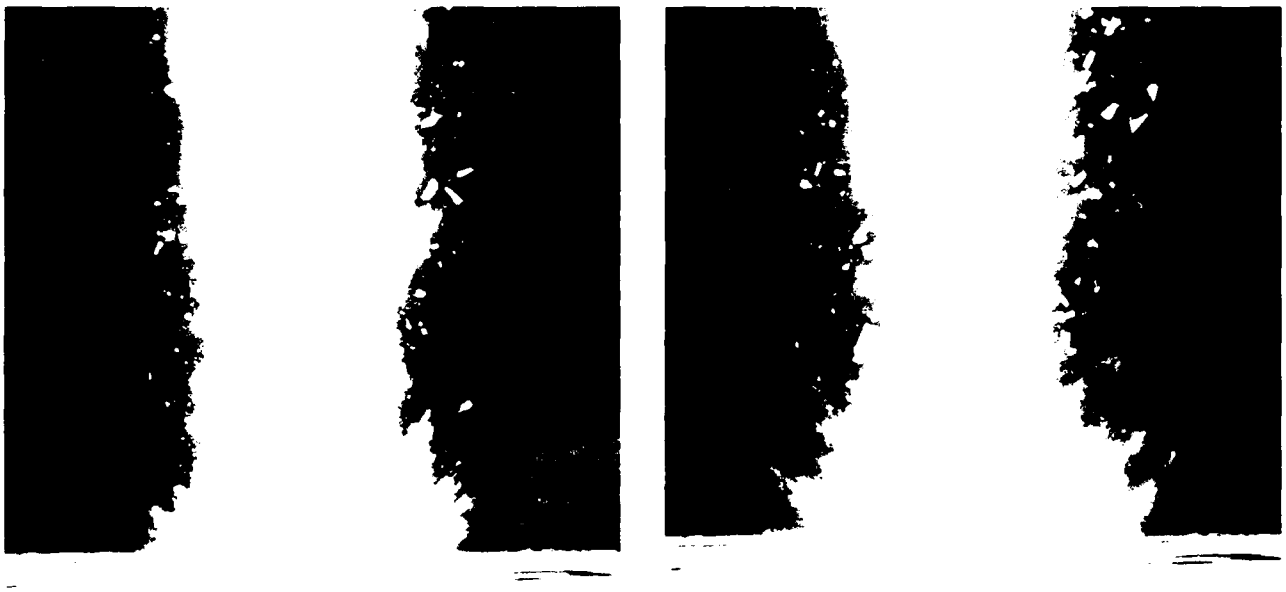

Figure A4 (cont'd).

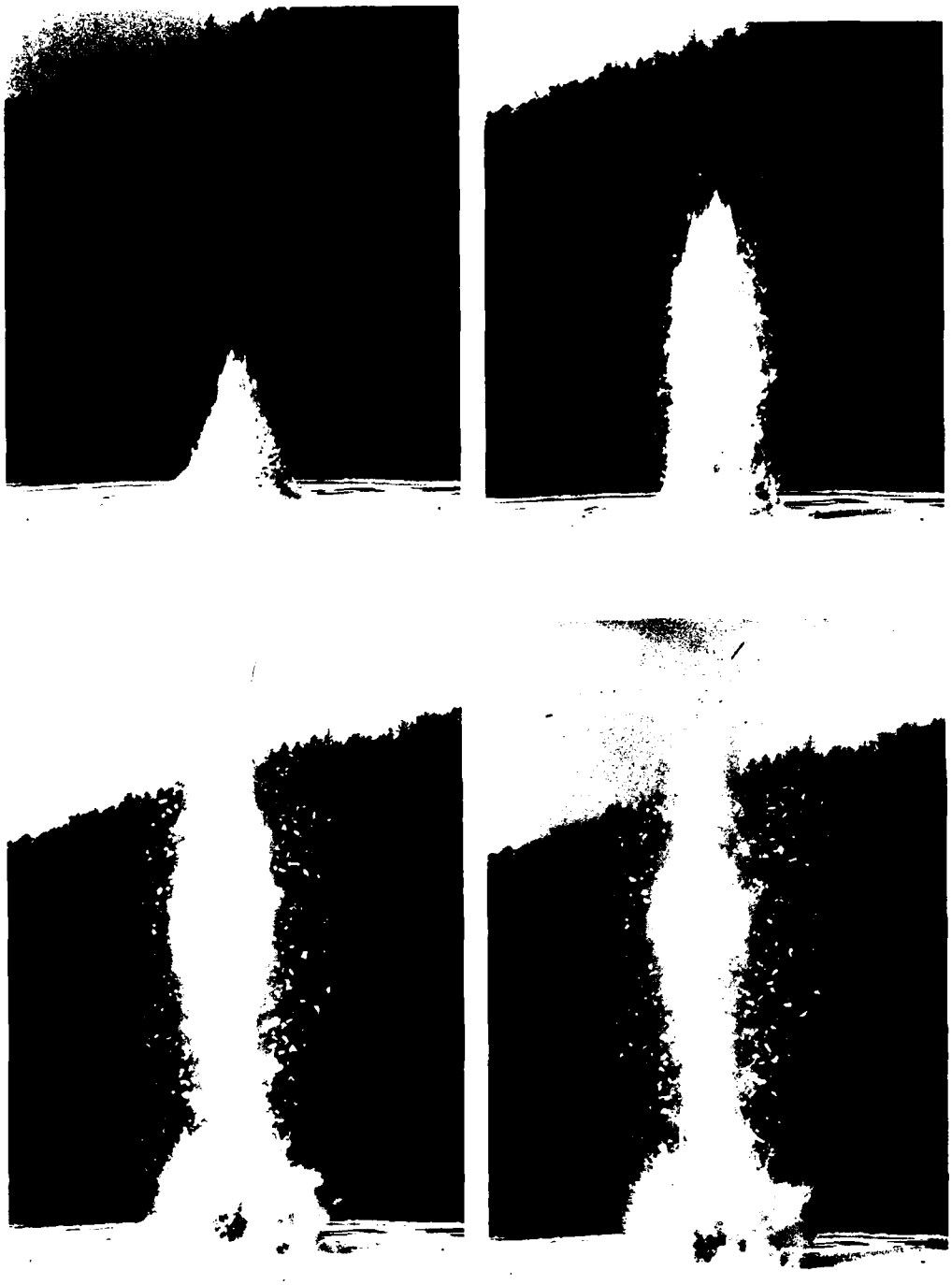

Figure A5. Six-frame sequence of shot no. 4 (camera no. 2).

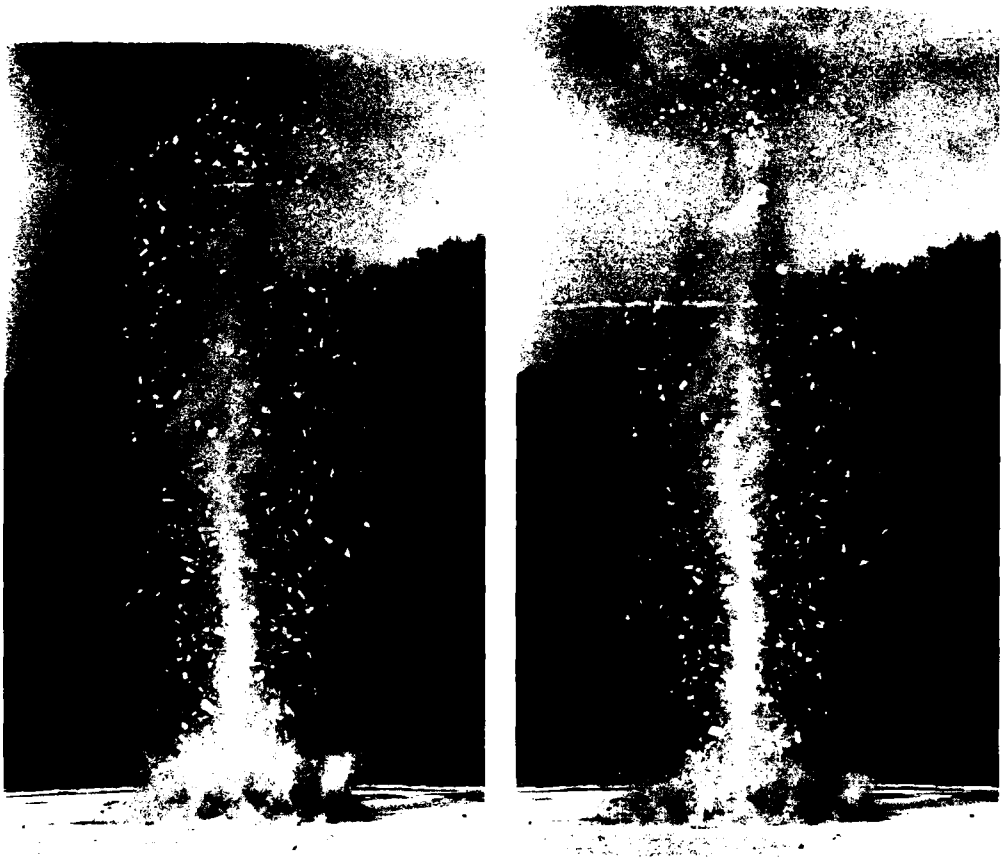

Figure A5 (cont'd).

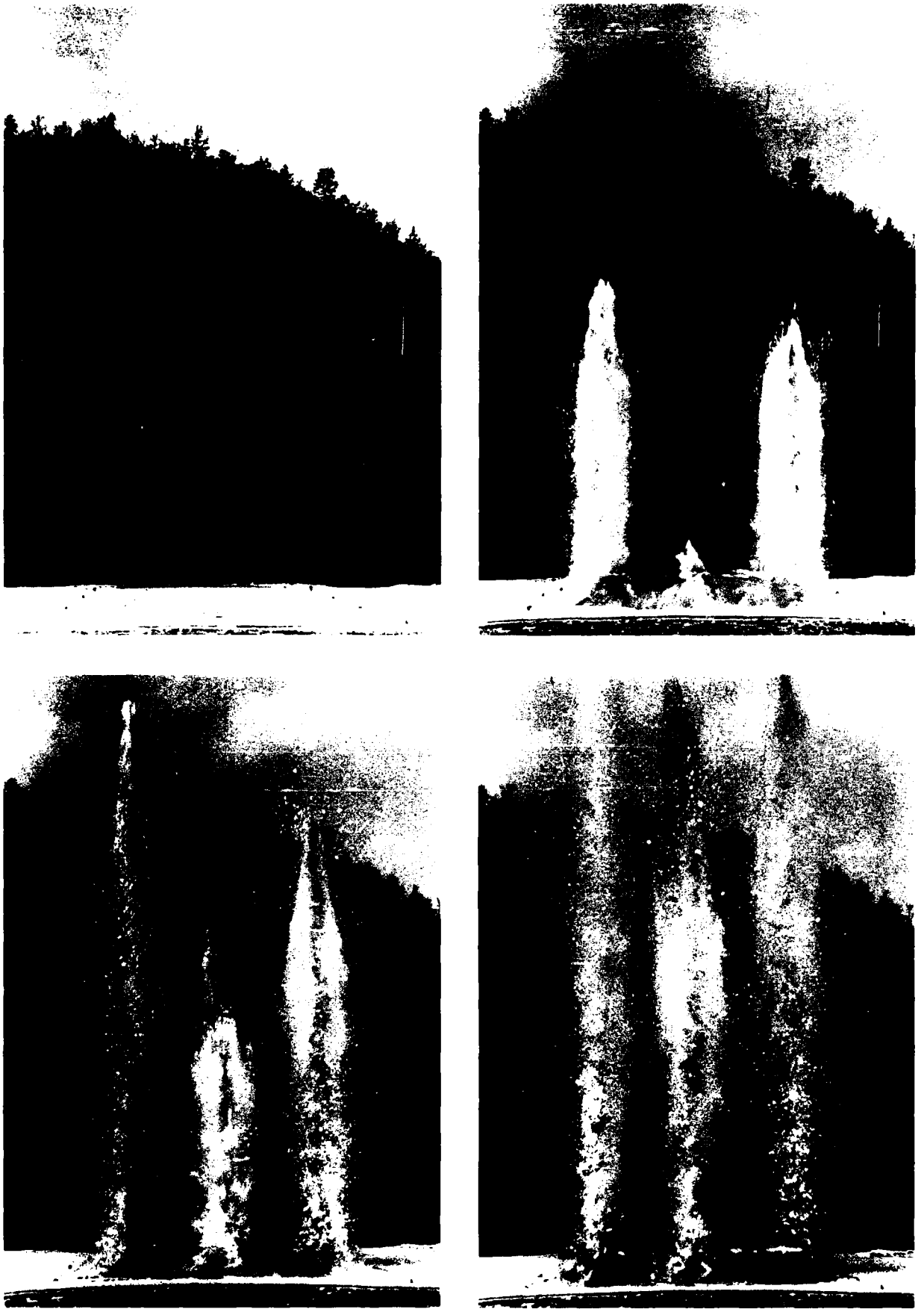

Figure A6. Six-frame sequence of shot no. 6.

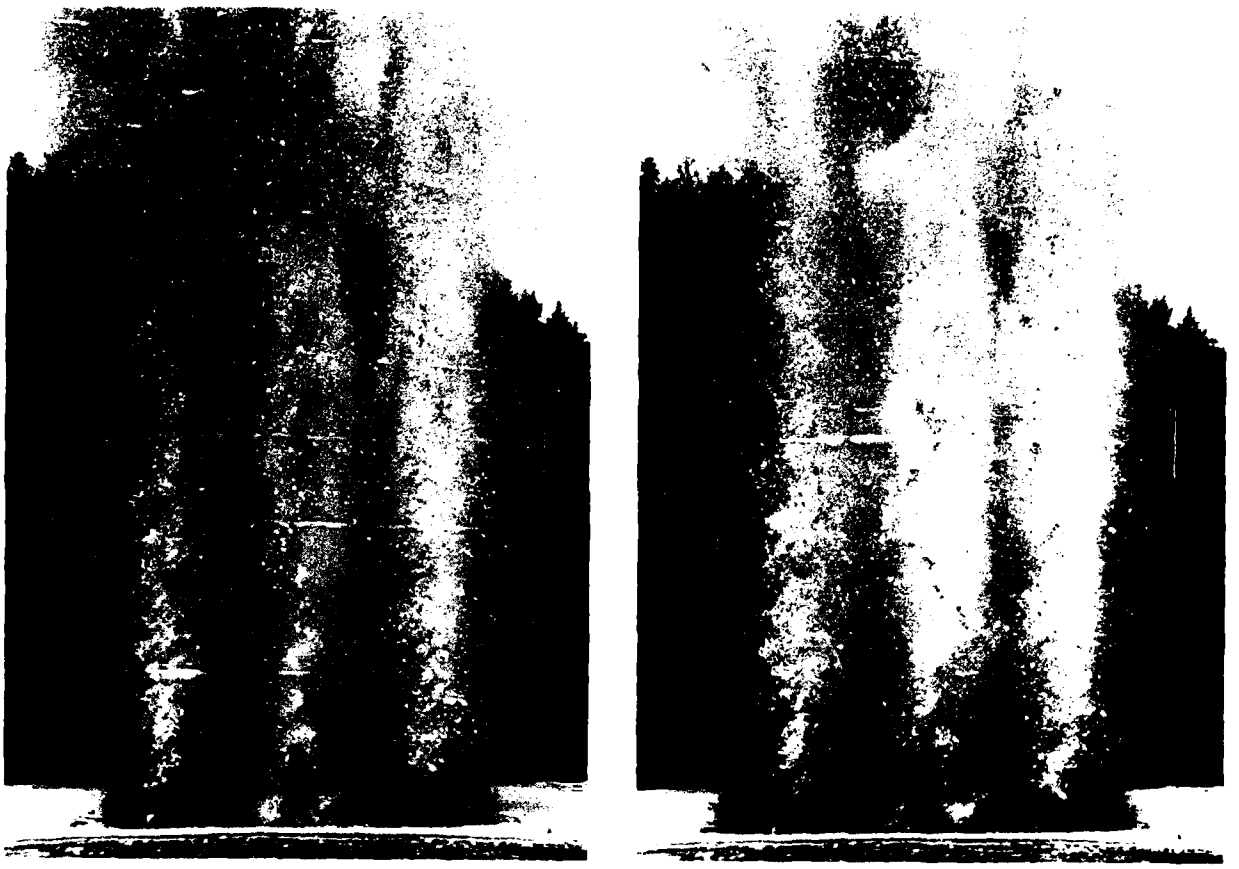

Figure A6 (cont'd).

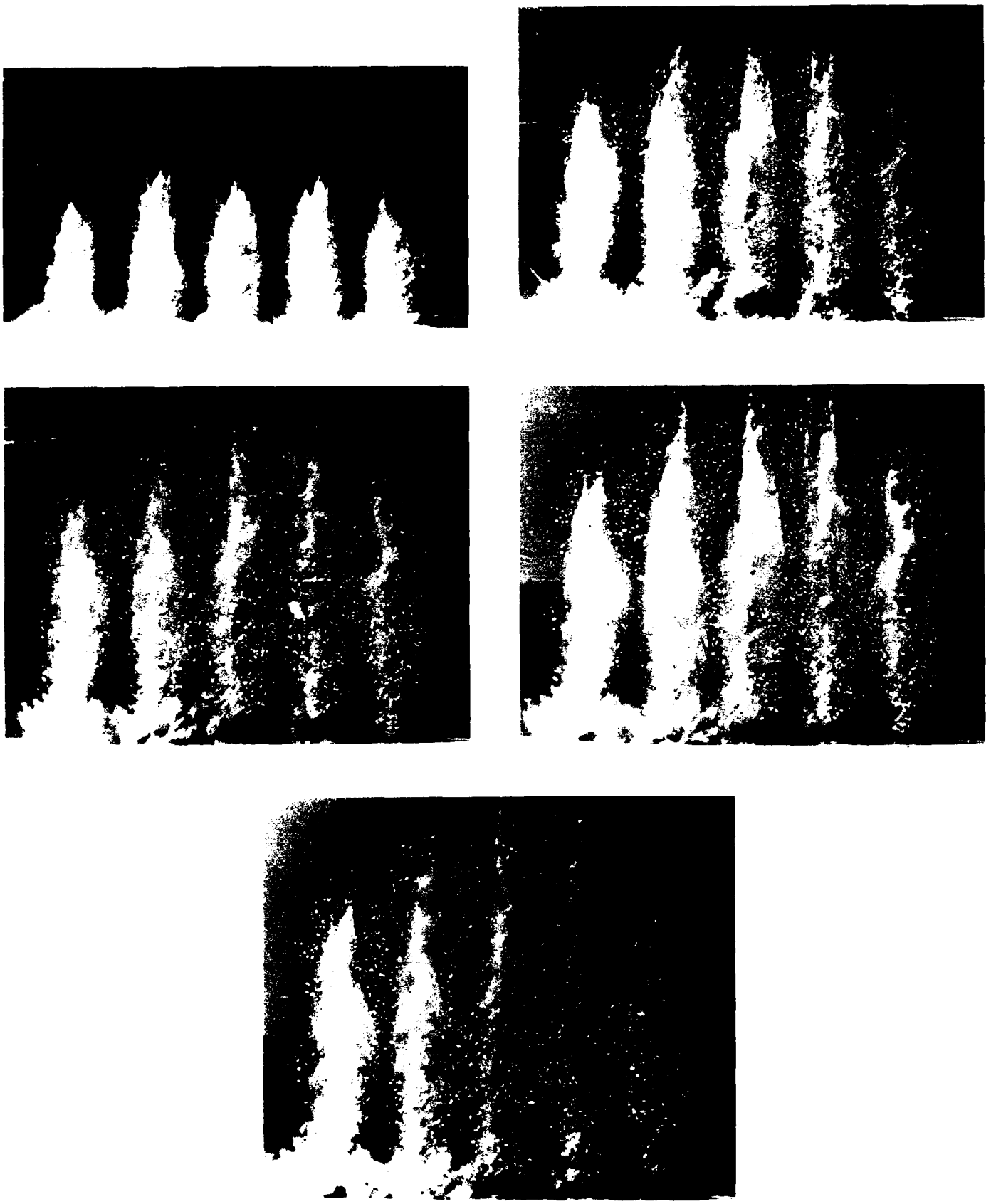

Figure A7. Seven-frame sequence of shot no. 7.

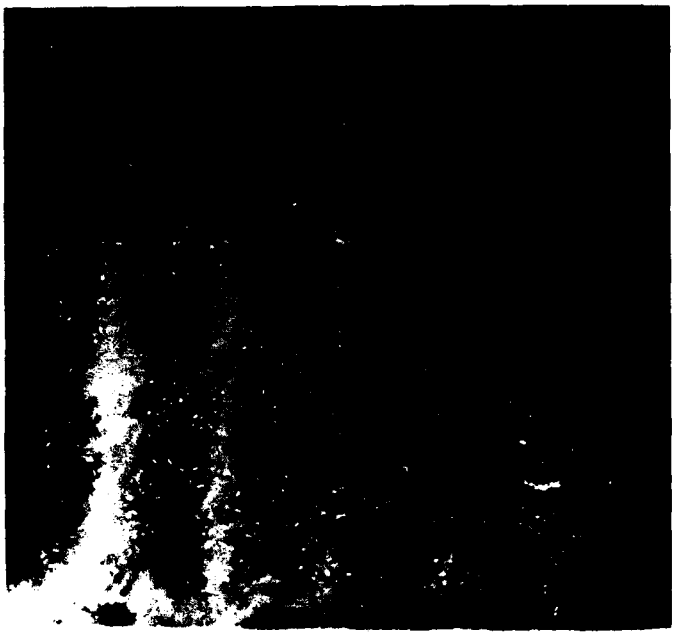

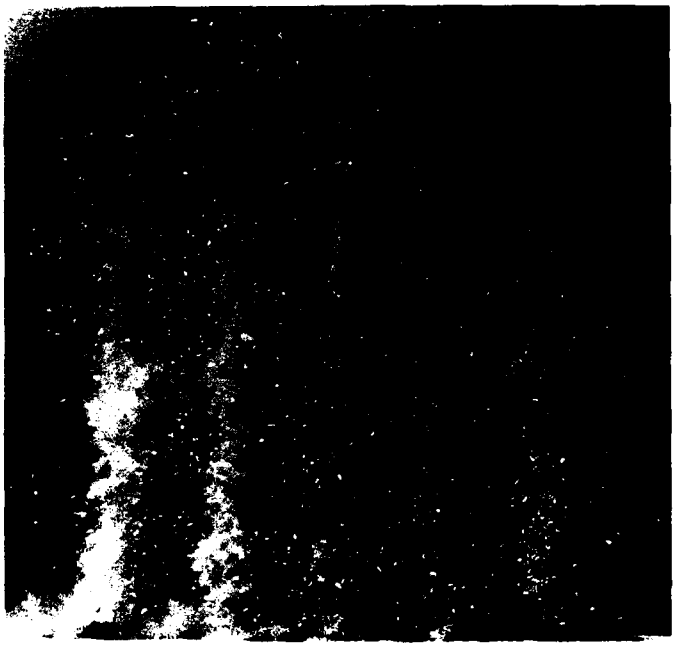

Figure A7 (cont'd).

APPENDIX B: VERTICAL DISPLACEMENT PLOTTED AGAINST TIME FOR THE VIDEO RECORDS

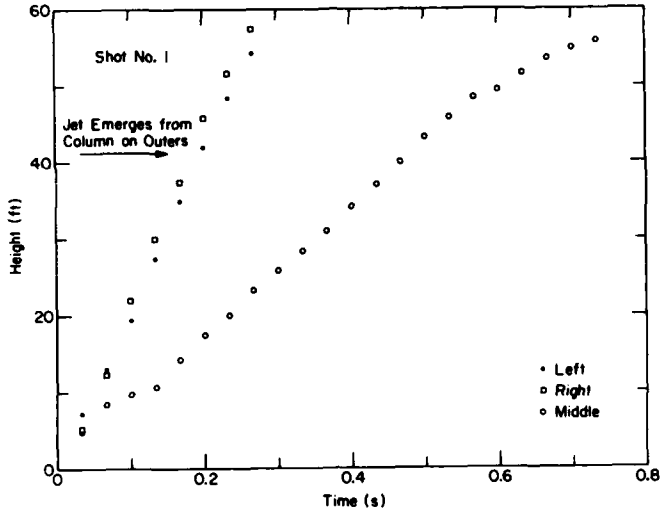

Figure B1. Data for shot no. 1.

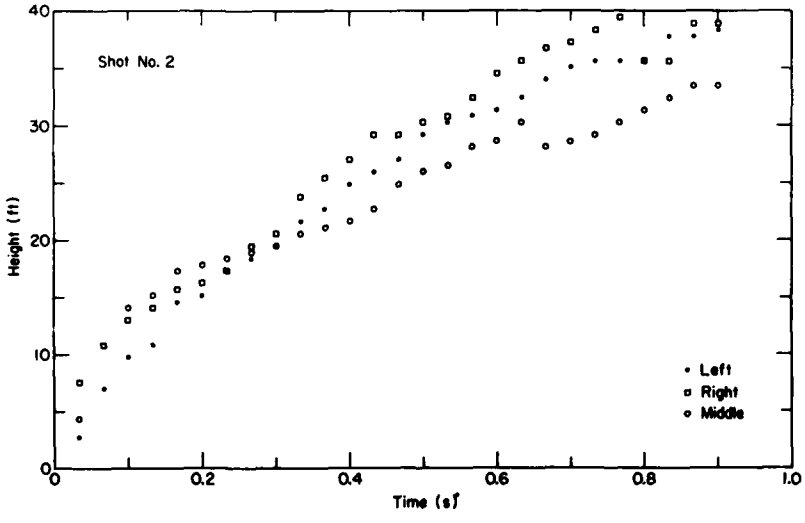

Figure B2. Data for shot no. 2 (the break in the trace for the middle explosion is caused by one part of the plume dying out and being overtaken by a more energetic spurt).

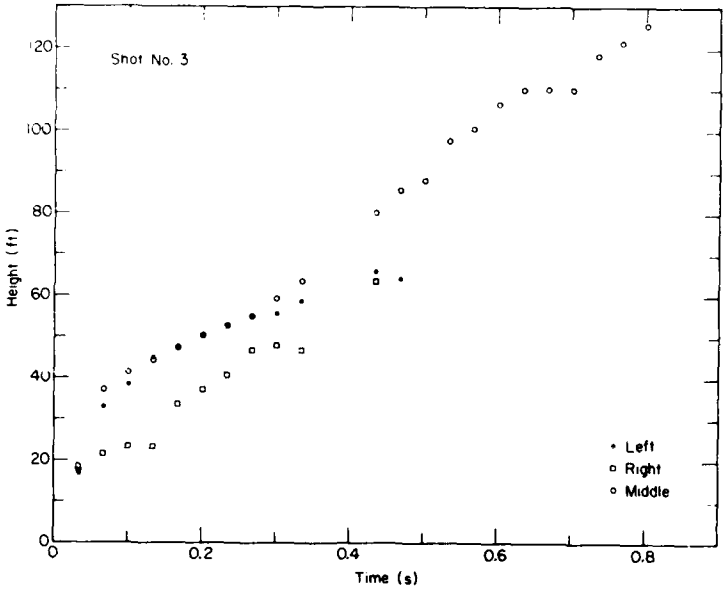

Figure B3. Data for shot no. 3 (the gap in this and other records is caused by loss of contrast in the video record).

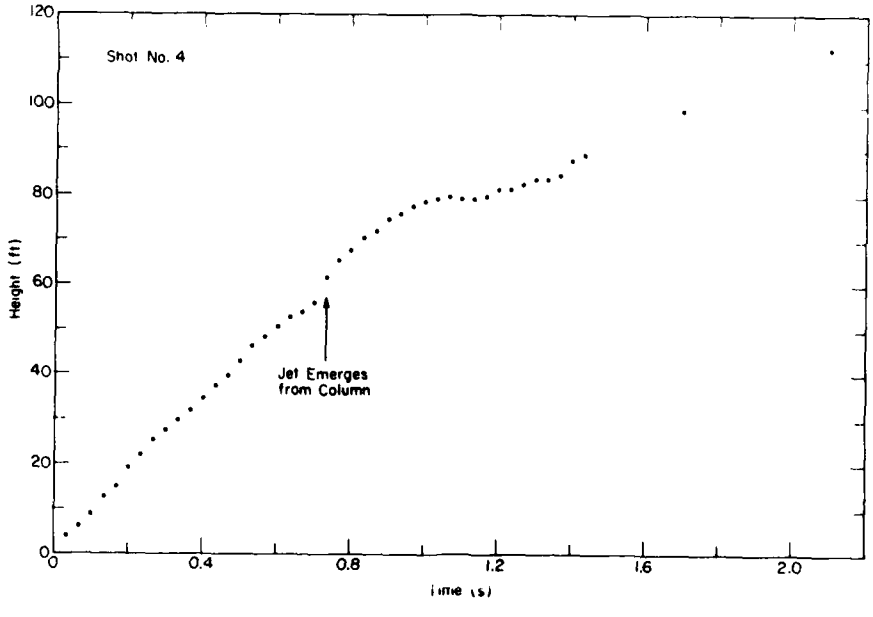

Figure B4. Data for shot no. 4.

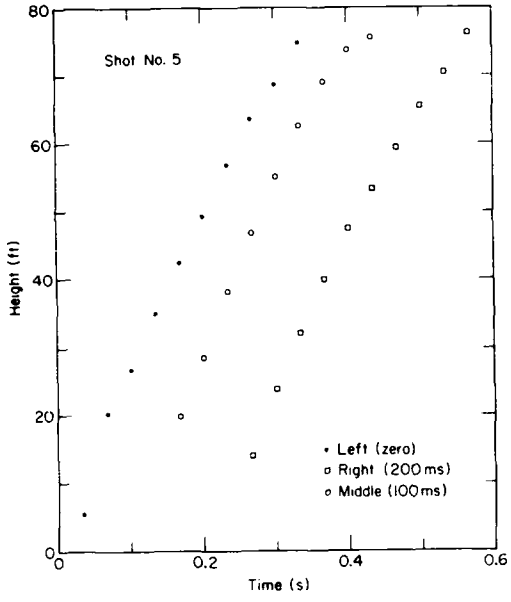

Figure B5. Data for shot no. 5.

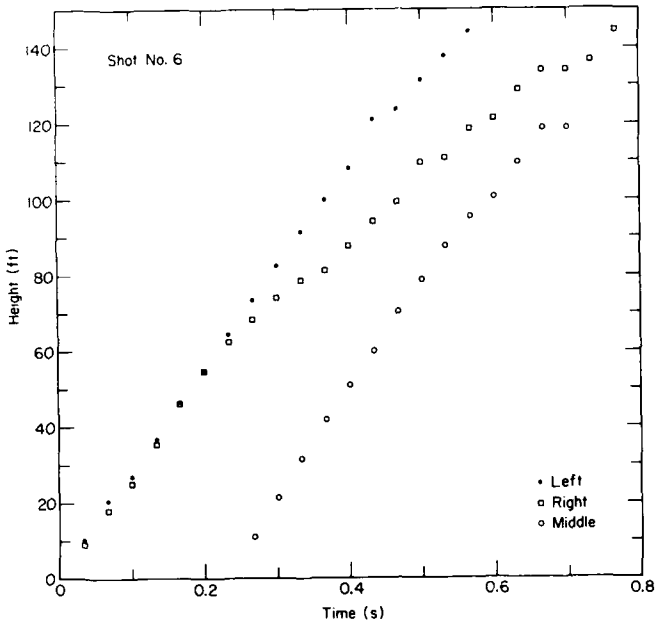

Figure B6. Data for shot no. 6.

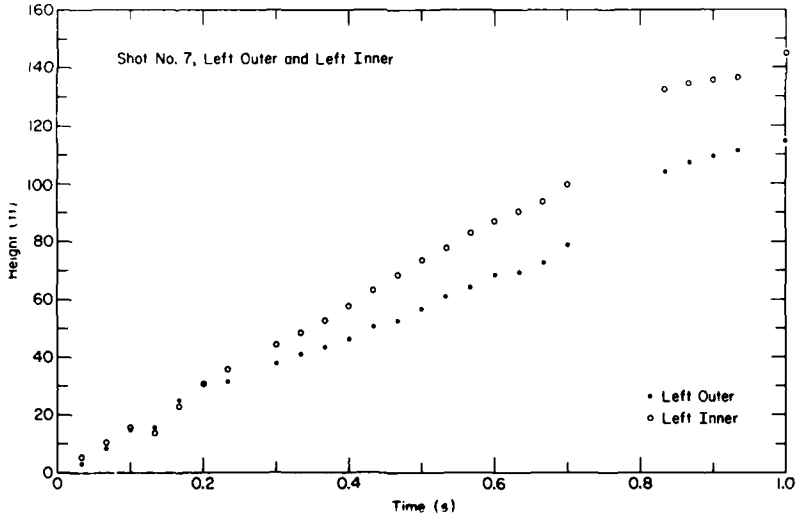

Figure B7. Data for right outer and right inner of shot no. 7.

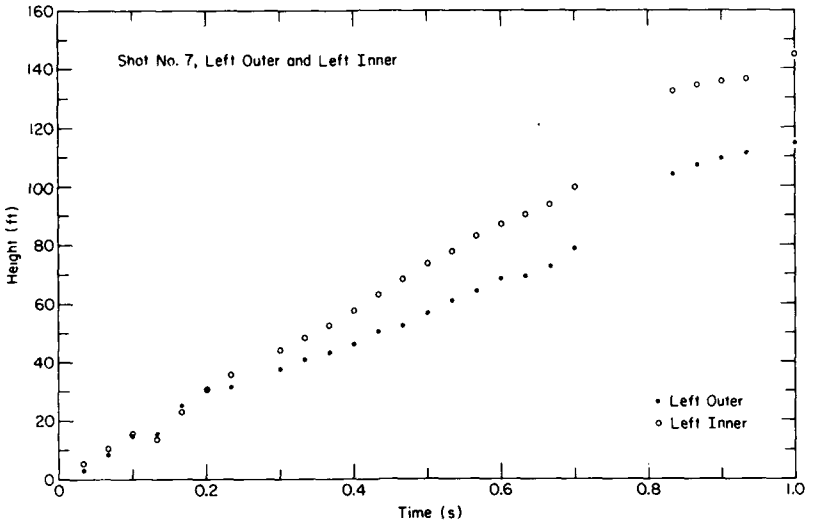

Figure B8. Data for left outer and left inner of shot no. 7.

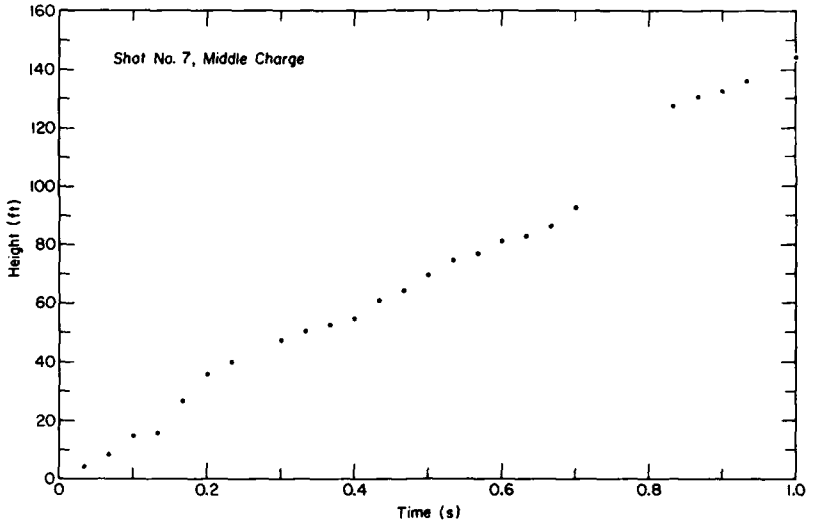

Figure B9. Data for middle charge of shot no. 7.